ACS APPLIED MATERIALS & INTERFACES

Research Article

www.acsami.org

Tunable Indirect to Direct Band Gap Transition of Monolayer Sc_2CO_2 by the Strain Effect

Youngbin Lee, Sung Beom Cho, and Yong-Chae Chung*

Department of Materials Science and Engineering, Hanyang University, Seoul 133-791, Korea

Supporting Information

ABSTRACT: MXene has not yet been investigated in optical applications because it is a newly suggested two-dimensional material. In the present work, the first investigation of the prospects of MXene as a novel optical nanodevice was done by applying strain to monolayer Sc_2CO_2 using first-principles density-functional theory. This single-layer material experiences an indirect to direct band gap transition with variation of the band gap size at a relatively small critical strain of about 2%. The present work emphasizes that monolayer MXene can become a promising material for an optical nanodevice by modulating the band gap properties using strain engineering.

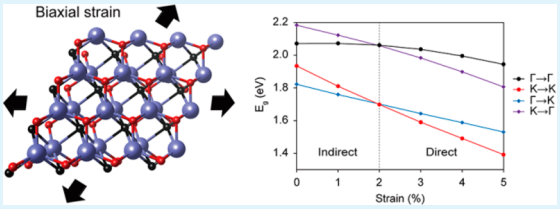

KEYWORDS: *MXene, Sc_2CO_2, indirect to direct band gap transition, strain, optical nanodevice, DFT*

INTRODUCTION

Experimentally successful separation of monolayer graphene and its remarkable characteristics have prompted substantial interest in diverse two-dimensional nanostructures.[1−5] Recently, among such graphene-like materials, Ti, V, Nb, and Ta carbides have been successfully fabricated as a single layer such as Ti_2C, Ti_3C_2, V_2C, Nb_2C, and Ta_4C_3.[6−10] Synthesis of these products is achieved from MAX phases by selective etching of the A layers and sonication, and they are comprised of alternate layers of a transition metal and carbon or nitrogen.[11,12] These new layered materials derived from their counterpart MAX phases are called MXene. Monolayer MXene generally has various common features such as metallic materials, high selectivity to intercalants, a higher elastic constant (c_{11}) than MAX bulk, and a larger bending rigidity than graphene due to the $(2n + 1)$ atomic layers.[12−15] Because most MXenes, except for some carbides mentioned above, have not yet been experimentally synthesized, simulations of their properties have received considerable attention for diverse applications such as electronic devices, electrochemical energy storage materials, a hydrogen storage medium, spintronic devices, and catalysts.[16−23]

From previous theoretical studies, it is known that most MXenes, which can be applied in the fields mentioned above, are metallic with the absence of a band gap in the bare condition.[24,25] This fact gives rise to the critical problem that bare MXene cannot be used for semiconducting or optical nanodevices. However, in a real etching process, functional groups like F, OH, O, or H bind to both sides of MXene.[12,26,27] Although most of these terminated MXenes still have metallic features, six types of terminated MXene have a band gap: Ti_2CO_2, Zr_2CO_2, Hf_2CO_2, Sc_2CO_2, $Sc_2C(OH)_2$, and Sc_2CF_2.[12,24] These semiconducting terminated MXenes have a Seebeck coefficient comparable to that of $SrTiO_3$, which has a large Seebeck coefficient (850 μV/K around 90 K), so they have been identified as promising thermoelectric devices.[12,24,25,28] However, problems using MXene in optics still exist because all semiconducting terminated MXenes except for $Sc_2C(OH)_2$ have an indirect band gap, which interrupts efficient light emission, and $Sc_2C(OH)_2$ has a relatively small direct band gap for optical devices.[24]

Generally, it is well-known that applying strain can be used to modify electronic properties, including an indirect band gap.[29−35] This is especially significant for two-dimensional materials because they can endure great tensile strain. Strain applied on such monolayer materials changes the interatomic distances and the relative positions of the atoms, which influences the electronic structure, and this effect can easily occur by a lattice mismatch on the substrate or mechanical loading.[33] Therefore, it is necessary to investigate the effect of strain on the band gap characteristics of semiconducting terminated MXene for useful optical devices.

In this article, the possibility of an indirect to direct band gap transition in MXene for outstanding optical nanodevices was examined by the strain effect on monolayer Sc_2CO_2 using first-principles density-functional theory (DFT) calculations. It is supposed that monolayer Sc_2CO_2 can be synthesized from bulk Sc_2InC among the MAX phases, and here, it was used because it has the largest band gap among the six semiconducting terminated MXenes.[24,36] Also, all strains in this work were applied equibiaxially along the *xy* plane. From this first exploration to use monolayer MXene in optics, it is expected that a wider choice for novel optical devices will be facilitated out of pre-existing nanomaterials.

Received: June 30, 2014
Accepted: August 8, 2014
Published: August 8, 2014

CALCULATION METHOD

DFT calculations were implemented using the Vienna Ab-initio Simulation Package (VASP) code.[37−39] All calculations were conducted under the Perdew−Burke−Ernzerhof (PBE)[40] generalized gradient approximation (GGA) with a projector augmented wave (PAW) pseudopotential method[41] for the exchange-correlation functional. A plane wave basis was set with an energy cutoff of 500 eV, and a 12 × 12 × 1 Gamma centered Monkhorst−Pack[42] k-point mesh was used for the Brillouin zone integrations. The atomic positions were relaxed using the conjugate gradient method and optimized until all the Hellmann−Feynman forces on any atom became less than 0.02 eV/Å. The criterion for energy convergence was 10^{-6} eV/cell. A Methfessel−Paxton smearing scheme was used with a width of 0.1 eV, and the density of states was calculated using a 24 × 24 × 1 Gamma centered Monkhorst−Pack k-point grid. The present work did not consider the spin−orbit coupling effect because the results of this study were negligibly affected by the effect.

Although MXene exfoliation has not been entirely understood yet, to simulate monolayer Sc_2CO_2, the system was used with a vacuum spacing of 25 Å because the length is enough to avoid an interaction between the layered MXene. As shown in Figure S1 (Supporting Information), the unit cell of the monolayer Sc_2CO_2 can be modeled as four types of hexagonal structures by the stacking position of the functional O atoms on both sides of Sc_2C, which consists of a C layer sandwiched between two Sc layers: Model 1 has two terminated O layers stacked on the same site with the opposite Sc layer with the C layer as the center; Model 2 has both terminated O layers stacked on the same site to the C layer; Model 3 has each terminated O layer located at the same positions in Models 1 and 2, respectively; Model 4 has two terminated O layers directly stacked on the top of the Sc layer on the same side.[24] The unit cells of each model were decided carefully by an energy convergence test. From these results, the lattice parameters of the most stable unit cells were 3.24, 3.38, 3.44, and 3.50 Å at Models 1, 2, 3, and 4, respectively (Figure S1, Supporting Information).

RESULTS AND DISCUSSION

Among these four types of models, according to the position of the O terminations, the most stable structure of monolayer Sc_2CO_2 is Model 3, as shown in Figure 1. As mentioned previously, the lattice parameter of this unit cell is 3.44 Å. To confirm the changes of the band gap by the strain effect, we applied biaxial tensile strain from 1 to 5% with reference to the optimized lattice parameter of Model 3. Prior to verifying the band gap properties in these strained single-layer structures, the total energies of each model of monolayer Sc_2CO_2 at 0 to 5% tensile strained states were calculated first to ascertain the most stable model at these conditions (Figure S2, Supporting Information), and these results show that the total energies of Model 3 are the lowest at all the strained lattice parameters. This means that Model 3 is preserved as the most stable configuration among the four models by tensile strain. Thus, the band gap characteristics of the strained monolayer Sc_2CO_2 were investigated only in Model 3.

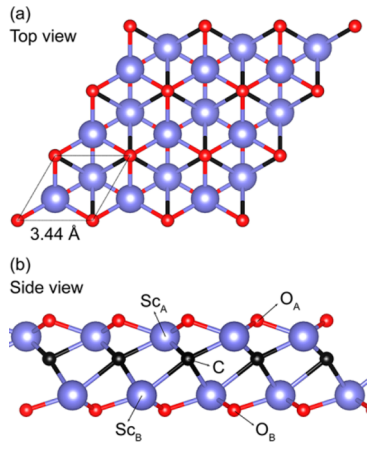

Figure 1. (a) Top view and (b) side view of the most stable configuration of monolayer Sc_2CO_2.

To confirm the band gap characters of these strained monolayer Sc_2CO_2, we present the band structures under each strain in Figure 2a. Originally, monolayer Sc_2CO_2 at the strain-free state has a Γ (valence band maximum, VBM) to K (conduction band minimum, CBM) indirect band gap of 1.82 eV. However, it changes to a K to K direct band gap when the system is applied to more than 2% tensile strain. To precisely confirm the effect of the strain on the indirect to direct band gap transition, we calculated the Γ to Γ and K to K direct gaps and Γ to K and K to Γ indirect gaps of monolayer Sc_2CO_2 as a function of strain, and these are plotted in Figure 2b. In Figure 2b, the difference between the Γ to K indirect gap and the K to K direct gap is only 2 meV at 2% tensile strain. From this result, it can be seen that the critical point of the indirect to direct band gap transition in monolayer Sc_2CO_2 by tensile strain is about 2%. Furthermore, the value of the band gap decreases from 1.82 to 1.39 eV as the tensile strain increases, and the reduction of this value is more sensitive after the indirect to direct band gap transition in particular. Therefore, it can be concluded that the band gap size of monolayer Sc_2CO_2 can be modulated using strain engineering, and the intriguing indirect to direct band gap transition in this system suggests a potential method using MXene for the design of novel optical nanodevices as well as thermoelectric and spintronic devices, Li-ion batteries, supercapacitors, catalysts, and hydrogen storage materials that have been researched for general applications of MXene.[16−23,43−45]

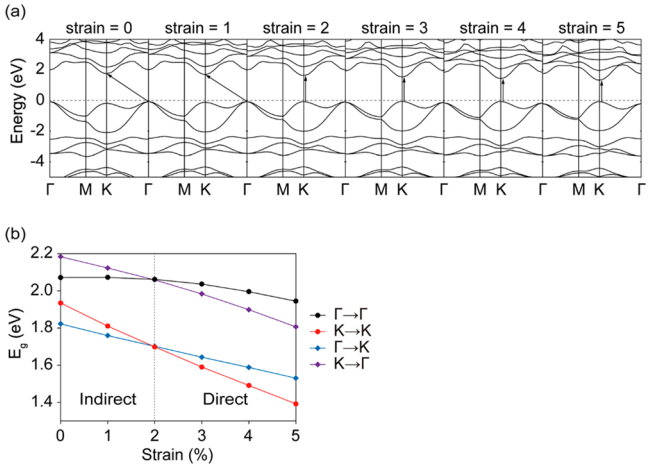

Figure 2. Change in the band gap in monolayer Sc_2CO_2 by tensile strain. (a) The band structures at each tensile strained state. The Fermi level was set to zero, and the arrows represent the directions of the band gap from the VBM to CBM states. (b) Change of energy gaps from the valence band to the conduction band as a function of strain; (black) Γ to Γ, (red) K to K, (blue) Γ to K, and (purple) K to Γ gaps.

To clarify the major factors related to these variations of the band gap properties, the contribution of each atom to the energy level in monolayer Sc_2CO_2 was first studied using the band structures, as shown in Figure 3. In these band structures,

dx.doi.org/10.1021/am504233d | ACS Appl. Mater. Interfaces 2014, 6, 14724−14728

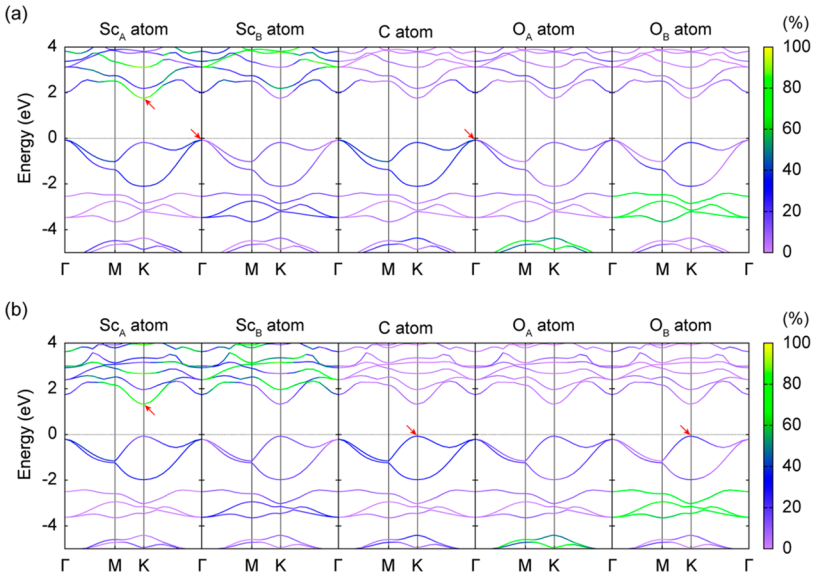

Figure 3. Contribution of each atom in monolayer Sc_2CO_2 to energy level at the (a) strain-free and (b) 5% tensile strained state. Percentages of the contributions of each atom are marked as a different color. The red arrows represent the VBM and CBM states at the band structure of the dominant atoms.

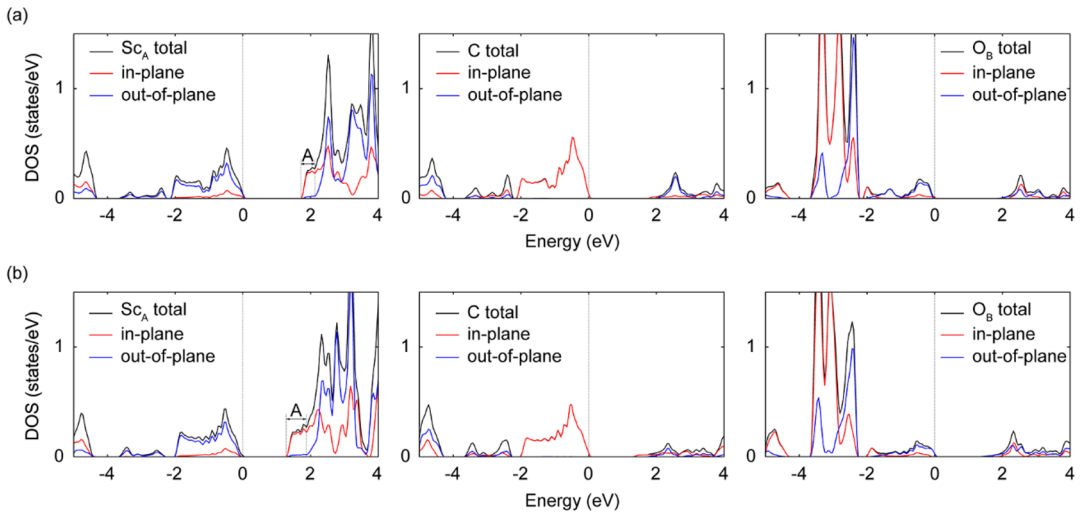

Figure 4. PDOS of the in-plane and out-of-plane orbitals in the Sc_A, C, and O_B atoms at the (a) strain-free and (b) 5% tensile strained states; (black) total, (red) in-plane, and (blue) out-of-plane orbitals in each atom. A region at the CBM in the Sc_A atom represents the energy range that is nearly related to the out-of-plane orbitals.

the cases of two Sc (Sc_A and Sc_B) and two O (O_A and O_B) atoms in a unit cell are considered separately because the most stable structure of the monolayer Sc_2CO_2 is asymmetric with the C layer as the center (Figure 1). First, in the strain-free state, the K point of the conduction band and the Γ point of the valence band are noticed as the CBM and VBM states (Figure 2). Among the five constituents of monolayer Sc_2CO_2 at the strain-free condition, the Sc_A atom mainly contributes to energy level at the CBM state as 88%, and energy level at the VBM state is primarily affected by the Sc_A and C atoms as 39 and 40%, respectively (Figure 3a). On the other hand, at a 5% tensile strained state which has a K to K direct band gap, it is confirmed that while the energy level at the CBM state still originates from the Sc_A atom as 85%, the C and O_B atoms are the dominant factors of energy level at the VBM state as 35 and 25%, respectively (Figure 3b). From these results, the Sc_A, C, and O_B atoms can be regarded as the major atoms that determine the band gap characters.

To understand the origin of the changes in the band gap characteristics in more detail, the partial density of states (PDOS) of these three components are presented in Figure 4. Generally, among the band gap properties, two elements, direction and size, are important for the optical nanodevices. First, in case of the band gap direction, it is altered from the Γ to K gap to K to K gap at tensile strain of about 2%. As mentioned in the previous paragraph, by indirect to direct band gap transition in monolayer Sc_2CO_2, while the major atom of the CBM state is maintained, main atoms of the VBM state are changed from the Sc_A and C to the O_B and C atoms according to point transition from the Γ to K. In addition, it can be obtained from the PDOS that the Sc_A and O_B atoms in the topmost valence band are strongly influenced by the out-of-plane orbitals. On the basis of these facts, indirect to direct

dx.doi.org/10.1021/am504233d | ACS Appl. Mater. Interfaces 2014, 6, 14724−14728

band gap transition by tensile strain results from the variation from the out-of-plane orbitals of the Sc_A atom to those of the O_B atom at the VBM state. Next, to investigate the cause of the alteration of size as other determinant of the band gap characters, we compared the PDOS at the strain-free state with those at the 5% tensile strained condition. As shown in Figure 4, the band gap size decreases as the A region increases, and the most varied orbital for this change is the in-plane orbitals of the Sc_A atom at the conduction band. Thus, it can be concluded that the primary factors of the variations of the band gap properties are the out-of-plane orbitals in the Sc_A (O_B) atoms at the Γ (K) point of the valence band and the in-plane orbitals in the Sc_A atom at the K point of the conduction band.

CONCLUSION

In summary, tuning the band gap characteristics of monolayer Sc_2CO_2 by the biaxial tensile strain effect for novel optical nanodevices was investigated using DFT calculations. From previous studies, it is well-known that strain on two-dimensional materials induces the changes of their electronic structures, and monolayer Sc_2CO_2 used in this work also faces these alterations. As results from these variations, as tensile strain increases, monolayer Sc_2CO_2 undergoes an indirect to direct band gap transition at a relatively small critical tensile strain of about 2%. In addition, the increase of tensile strain from 0 to 5% leads to a gradual reduction of the band gap size in this system. From these results, it can be concluded that the band gap of monolayer Sc_2CO_2 can be modulated to have attractive features in the optics by strain. Therefore, we suggest a practical route to modify the band gap properties of monolayer MXene using strain engineering for potential optical nanodevices.

ASSOCIATED CONTENT

Supporting Information

Geometric properties of monolayer Sc_2CO_2 according to the type of model; most stable model of monolayer Sc_2CO_2 at the strained states; and main factors of the band gap properties in monolayer Sc_2CO_2. This material is available free of charge via the Internet at http://pubs.acs.org.

AUTHOR INFORMATION

Corresponding Author

*E-mail: yongchae@hanyang.ac.kr, Tel.: +82-2-2220-0507.

Notes

The authors declare no competing financial interest.

ACKNOWLEDGMENTS

This research was supported by the Basic Science Research Program through the National Research Foundation of Korea (NRF) funded by the Ministry of Education (2013R1A1A2A10064432).

REFERENCES

(1) Geim, A. K. Graphene: Status and Prospects. *Science* **2009**, *324*, 1530−1534.
(2) Geim, A. K.; Novoselov, K. S. The Rise of Graphene. *Nat. Mater.* **2007**, *6*, 183−191.
(3) Tang, Q.; Zhou, Z. Graphene-Analogous Low-Dimensional Materials. *Prog. Mater. Sci.* **2013**, *58*, 1244−1315.
(4) Zhang, X.; Xie, Y. Recent Advances in Free-Standing Two-Dimensional Crystals with Atomic Thickness: Design, Assembly, and Transfer Strategies. *Chem. Soc. Rev.* **2013**, *42*, 8187−8199.
(5) Koski, K. J.; Cui, Y. The New Skinny in Two-Dimensional Nanomaterials. *ACS Nano* **2013**, *7*, 3739−3743.
(6) Naguib, M.; Kurtoglu, M.; Presser, V.; Lu, J.; Niu, J.; Heon, M.; Hultman, L.; Gogotsi, Y.; Barsoum, M. W. Two-Dimensional Nanocrystals Produced by Exfoliation of Ti_3AlC_2. *Adv. Mater.* **2011**, *23*, 4248−4253.
(7) Naguib, M.; Mashtalir, O.; Carle, J.; Presser, V.; Lu, J.; Hultman, L.; Gogotsi, Y.; Barsoum, M. W. Two-Dimensional Transition Metal Carbides. *ACS Nano* **2012**, *6*, 1322−1331.
(8) Naguib, M.; Halim, J.; Lu, J.; Cook, K. M.; Hultman, L.; Gogotsi, Y.; Barsoum, M. W. New Two-Dimensional Niobium and Vanadium Carbides as Promising Materials for Li-Ion Batteries. *J. Am. Chem. Soc.* **2013**, *135*, 15966−15969.
(9) Chang, F.; Li, C.; Yang, J.; Tang, H.; Xue, M. Synthesis of a New Graphene-like Transition Metal Carbide by De-Intercalating Ti_3AlC_2. *Mater. Lett.* **2013**, *109*, 295−298.
(10) Mashtalir, O.; Naguib, M.; Dyatkin, B.; Gogotsi, Y.; Barsoum, M. W. Kinetics of Aluminum Extraction from Ti_3AlC_2 in Hydrofluoric Acid. *Mater. Chem. Phys.* **2013**, *139*, 147−152.
(11) Ivanovskii, A. L.; Enyashin, A. N. Graphene-like Transition-Metal Nanocarbides and Nanonitrides. *Russ. Chem. Rev.* **2013**, *82*, 735−746.
(12) Naguib, M.; Mochalin, V. N.; Barsoum, M. W.; Gogotsi, Y. 25th Anniversary Article: MXenes: A New Family of Two-Dimensional Materials. *Adv. Mater.* **2014**, *26*, 992−1005.
(13) Lukatskaya, M. R.; Mashtalir, O.; Ren, C. E.; Dall'Agnese, Y.; Rozier, P.; Taberna, P. L.; Naguib, M.; Simon, P.; Barsoum, M. W.; Gogotsi, Y. Cation Intercalation and High Volumetric Capacitance of Two-Dimensional Titanium Carbide. *Science* **2013**, *341*, 1502−1505.
(14) Mashtalir, O.; Naguib, M.; Mochalin, V. N.; Dall'Agnese, Y.; Heon, M.; Barsoum, M. W.; Gogotsi, Y. Intercalation and Delamination of Layered Carbides and Carbonitrides. *Nat. Commun.* **2013**, *4*, 1716.
(15) Wang, S.; Li, J.-X.; Du, Y.-L.; Cui, C. First-Principles Study on Structural, Electronic and Elastic Properties of Graphene-like Hexagonal Ti_2C Monolayer. *Comput. Mater. Sci.* **2014**, *83*, 290−293.
(16) Tang, Q.; Zhou, Z.; Shen, P. Are MXenes Promising Anode Materials for Li Ion Batteries? Computational Studies on Electronic Properties and Li Storage Capability of Ti_3C_2 and $Ti_3C_2X_2$ (X = F, OH) Monolayer. *J. Am. Chem. Soc.* **2012**, *134*, 16909−16916.
(17) Shein, I.; Ivanovskii, A. Graphene-like Titanium Carbides and Nitrides $Ti_{n+1}C_n$, $Ti_{n+1}N_n$ (n = 1, 2, and 3) from De-Intercalated MAX Phases: First-Principles Probing of Their Structural, Electronic Properties and Relative Stability. *Comput. Mater. Sci.* **2012**, *65*, 104−114.
(18) Gan, L.-Y.; Zhao, Y.-J.; Huang, D.; Schwingenschlögl, U. First-Principles Analysis of MoS_2/Ti_2C and MoS_2/Ti_2CY_2 (Y = F and OH) All-2D Semiconductor/Metal Contacts. *Phys. Rev. B* **2013**, *87*, 245307.
(19) Hu, Q.; Sun, D.; Wu, Q.; Wang, H.; Wang, L.; Liu, B.; Zhou, A.; He, J. MXene: A New Family of Promising Hydrogen Storage Medium. *J. Phys. Chem. A* **2013**, *117*, 14253−14260.
(20) Lane, N. J.; Barsoum, M. W.; Rondinelli, J. M. Correlation Effects and Spin-Orbit Interactions in Two-Dimensional Hexagonal 5d Transition Metal Carbides, $Ta_{n+1}C_n$ (n = 1, 2, 3). *EPL* **2013**, *101*, 57004.
(21) Xie, Y.; Naguib, M.; Mochalin, V. N.; Barsoum, M. W.; Gogotsi, Y.; Yu, X.; Nam, K.-W.; Yang, X.-Q.; Kolesnikov, A. I.; Kent, P. R. Role of Surface Structure on Li-Ion Energy Storage Capacity of Two-Dimensional Transition Metal Carbides. *J. Am. Chem. Soc.* **2014**, *136*, 6385−6394.
(22) Peng, X.; Peng, L.; Wu, C.; Xie, Y. Two Dimensional Nanomaterials for Flexible Supercapacitors. *Chem. Soc. Rev.* **2014**, *43*, 3303−3323.
(23) Ma, Z.; Hu, Z.; Zhao, X.; Tang, Q.; Wu, D.; Zhou, Z.; Zhang, L. Tunable Band Structures of Heterostructured Bilayers with Transition-Metal Dichalcogenide and MXene Monolayer. *J. Phys. Chem. C* **2014**, *118*, 5593−5599.
(24) Khazaei, M.; Arai, M.; Sasaki, T.; Chung, C.-Y.; Venkataramanan, N. S.; Estili, M.; Sakka, Y.; Kawazoe, Y. Novel

Electronic and Magnetic Properties of Two-Dimensional Transition Metal Carbides and Nitrides. *Adv. Funct. Mater.* **2013**, *23*, 2185−2192.
(25) Khazaei, M.; Arai, M.; Sasaki, T.; Estili, M.; Sakka, Y. Two-Dimensional Molybdenum Carbides: Potential Thermoelectric Materials of the MXene Family. *Phys. Chem. Chem. Phys.* **2014**, *16*, 7841−7849.
(26) Enyashin, A.; Ivanovskii, A. Two-Dimensional Titanium Carbonitrides and Their Hydroxylated Derivatives: Structural, Electronic Properties, and Stability of MXenes $Ti_3C_{2-x}N_x(OH)_2$ from DFTB Calculations. *J. Solid State Chem.* **2013**, *207*, 42−48.
(27) Enyashin, A. N.; Ivanovskii, A. L. Structural and Electronic Properties and Stability of MXenes Ti_2C and Ti_3C_2 Functionalized by Methoxy Groups. *J. Phys. Chem. C* **2013**, *117*, 13637−13643.
(28) Ohta, H.; Kim, S.; Mune, Y.; Mizoguchi, T.; Nomura, K.; Ohta, S.; Nomura, T.; Nakanishi, Y.; Ikuhara, Y.; Hirano, M.; Hosono, H.; Koumoto, K. Giant Thermoelectric Seebeck Coefficient of a Two-Dimensional Electron Gas in $SrTiO_3$. *Nat. Mater.* **2007**, *6*, 129−134.
(29) Zhong, X.; Yap, Y. K.; Pandey, R.; Karna, S. P. First-Principles Study of Strain-Induced Modulation of Energy Gaps of Graphene/BN and BN Bilayers. *Phys. Rev. B* **2011**, *83*, 193403.
(30) Yun, W. S.; Han, S.; Hong, S. C.; Kim, I. G.; Lee, J. Thickness and Strain Effects on Electronic Structures of Transition Metal Dichalcogenides: 2H-MX_2 Semiconductors (M = Mo, W; X = S, Se, Te). *Phys. Rev. B* **2012**, *85*, 033305.
(31) Lu, P.; Wu, X.; Guo, W.; Zeng, X. C. Strain-Dependent Electronic and Magnetic Properties of MoS_2 Monolayer, Bilayer, Nanoribbons and Nanotubes. *Phys. Chem. Chem. Phys.* **2012**, *14*, 13035−13040.
(32) Gupta, S.; Magyari-Köpe, B.; Nishi, Y.; Saraswat, K. C. Achieving Direct Band Gap in Germanium through Integration of Sn Alloying and External Strain. *J. Appl. Phys.* **2013**, *113*, 073707.
(33) Shi, H.; Pan, H.; Zhang, Y.-W.; Yakobson, B. I. Quasiparticle Band Structures and Optical Properties of Strained Monolayer MoS_2 and WS_2. *Phys. Rev. B* **2013**, *87*, 155304.
(34) Horzum, S.; Sahin, H.; Cahangirov, S.; Cudazzo, P.; Rubio, A.; Serin, T.; Peeters, F. Phonon Softening and Direct to Indirect Band Gap Crossover in Strained Single-Layer $MoSe_2$. *Phys. Rev. B* **2013**, *87*, 125415.
(35) Zhou, W.; Liu, Y.; Yang, Y.; Wu, P. Band Gap Engineering of SnO2 by Epitaxial Strain: Experimental and Theoretical Investigations. *J. Phys. Chem. C* **2014**, *118*, 6448−6453.
(36) Dahlqvist, M.; Alling, B.; Rosén, J. Stability Trends of MAX Phases from First Principles. *Phys. Rev. B* **2010**, *81*, 220102.
(37) Kresse, G.; Hafner, J. Ab Initio Molecular Dynamics for Liquid Metals. *Phys. Rev. B* **1993**, *47*, 558.
(38) Kresse, G.; Furthmüller, Jü. Efficiency of ab Initio Total Calculations Energy for Metals and Semiconductors Using a Plane-Wave Basis Set. *Comput. Mater. Sci.* **1996**, *6*, 15−50.
(39) Kresse, G.; Furthmüller, Jü. Efficient Iterative Schemes for Ab Initio Total-Energy Calculations Using a Plane-Wave Basis Set. *Phys. Rev. B* **1996**, *54*, 11169.
(40) Perdew, J. P.; Burke, K.; Ernzerhof, M. Generalized Gradient Approximation Made Simple. *Phys. Rev. Lett.* **1996**, *77*, 3865.
(41) Kresse, G.; Joubert, D. From Ultrasoft Pseudopotentials to the Projector Augmented-Wave Method. *Phys. Rev. B* **1999**, *59*, 1758.
(42) Monkhorst, H. J.; Pack, J. D. Special Points for Brillouin-Zone Integrations. *Phys. Rev. B* **1976**, *13*, 5188−5192.
(43) Naguib, M.; Come, J.; Dyatkin, B.; Presser, V.; Taberna, P.-L.; Simon, P.; Barsoum, M. W.; Gogotsi, Y. MXene: A Promising Transition Metal Carbide Anode for Lithium-Ion Batteries. *Electrochem. Commun.* **2012**, *16*, 61−64.
(44) Peng, Q.; Guo, J.; Zhang, Q.; Xiang, J.; Liu, B.; Zhou, A.; Liu, R.; Tian, Y. Unique Lead Adsorption Behavior of Activated Hydroxyl Group in Two-Dimensional Titanium Carbide. *J. Am. Chem. Soc.* **2014**, *136*, 4113−4116.
(45) Halim, J.; Lukatskaya, M. R.; Cook, K. M.; Lu, J.; Smith, C. R.; Naslund, L.-Å.; May, S. J.; Hultman, L.; Gogotsi, Y.; Eklund, P.; Barsoum, M. W. Transparent Conductive Two-Dimensional Titanium Carbide Epitaxial Thin Films. *Chem. Mater.* **2014**, *26*, 2374−2381.